Precise optical trap alignment using piezo-motorized mirrors

Enrico Jonas Huland

Bachelorarbeit in Physik
angefertigt im Institut für Angewandte Physik

vorgelegt der
Mathematisch-Naturwissenschaftlichen Fakultät
der
Rheinischen Friedrich-Wilhelms-Universität
Bonn

January 2026

Ich versichere, dass ich diese Arbeit selbstständig verfasst und keine anderen als die angegebenen Quellen und Hilfsmittel benutzt sowie die Zitate kenntlich gemacht habe.

Bonn, 21.01.2026 Ernie Haaland

Datum Unterschrift

Gutachter und Betreuer: Prof. Dr. Sebastian Hofferberth
Gutachter: Prof. Dr. Stefan Linden

Contents

CHAPTER 1

Introduction

The precision alignment of optical systems is a major requirement for modern cold atom and quantum computing related experiments. Depending on the use case, there are different requirements optical devices have to meet, like fast response time, high precision, long term stability or longevity. While a setup, that is actively stabilized or utilizes a live position change, will require a fast response time and a high steering speed, systems that are static in nature might require a high precision alignment with excellent long term stability. [1][2]

Optical dipole traps are a powerful tool for the trapping of ultracold atoms [3]. In the Rubidium Rydberg Quantum Optics experiment in the NQO group, ultracold Rubidium is trapped in a crossed optical dipole trap, formed by a single beam that is reflected to form a cross [4].

The alignment of this optical trap is extremely critical, as the trap has to be overlapped with the focus of the tightly focused probe beam [5]. The alignment of the optical trap is done with mirrors in high-precision adjustable mirror mounts. Before, the mounts were manually adjustable, but in the course of this thesis, the mounts were replaced with piezo-motorized mirror mounts in order to achieve a more precise and reproducible way to align our optical trap.

In this thesis, chapter 2 will focus on the piezo-motorized mirror mounts. Here, the detailed characteristics of the selected product are discussed and tested. Of particular interest is the alignment accuracy and the long term stability. Additionally we show, that the mirrors can be aligned freely and controlled in all directions.

In chapter 3 the alignment of the crossed optical trap is discussed in more detail. For this, the setup of the optical trap was reproduced in python with the help of the optiland package [6]. The concrete alignment process is covered in more detail with regard to the exchange of the optical dipole trap mirror mounts in the main experiment. Finally some of the simulation results are compared with measurements taken in the real experiment.

CHAPTER 2

Piezo motorized mirrors

Optomechanical mirror mounts are one of the most common components in every optics lab. They are usually used for the precise and reliable alignment of optical setups. The mechanical alignment precision of these mounts is dependent on the quality of machinery for mass production and the accuracy of the person responsible for the adjustment. Both of these factors hit their limit, when it comes to the precision required in modern cold atom experiments. For this purpose we went looking for alternative solutions, that offer remote controlled mirrors for reproducible alignment, with higher precision than comparable mounts with fine adjustment screws, as well as good passive stability.

While a mirror mount, that utilizes a single piezo crystal or a piezo stack, can in theory be used to achieve more precise control and finer adjustability, we decided on mirror mounts, that are based on the slip stick principle. The main advantage of mounts based on the slip and stick principle compared to a mount controlled directly by a piezo element, is that the piezo in the slip and stick motor is used to rotate a screw, which will then remain in place even if no voltage is applied to the piezo. A single piezo element on the other hand will require a permanent voltage to remain in position. [7]

In the following we will introduce the working principle and the specific mount we are using. The mirror tilting angle per single step of the piezo driven slip stick motor is of special interest to us, as that will give us the precision that can be used for the alignment of the optical trap. The tilting angle is different for forwards and backwards direction of the motor, which is why the angle will be measured for both directions (section 2.2). Furthermore the stability of the mirror mounts will be measured over a longer time interval, to ensure that the trap will not change significantly over time (section 2.4).

2.1 Working Principle

The piezo motors are inserted into the mirror mounts by a wide threaded screw in the same way fine threaded screws are installed in the mirror mounts, so one piezo motor will tilt the mirror around the horizontal axis, and the other around the vertical axis. The motors themselves directly turn a fine threaded screw that runs all the way through the outer wide threaded screw and the piezo motors. The piezo driven motors are addressed by an external controller, which generates a sawtooth signal and can be controlled from a computer which also enables procedures for automatic alignment [8].

2.1.1 Converse piezoelectric effect

When strain is applied to piezoelectric materials the mean charge distribution experiences a shift between positive and negative charges which results in a polarisation. This in turn can be observed by the resulting small electric field. The same effect also exists converse, meaning that an external electrical field will induce an internal polarisation of the material which will contract or expand the piezoelectric material. Piezo electricity can only appear in materials where the atoms of the unit cell are distributed without center of inversion. [9][10]

For small fields and strains, polarisation, strain, and electric field are proportional to each other. The resulting mechanical strain S from applying small electrical fields E can be calculated like this [11]:

$$S = s^E T + dE \ , \tag{2.1}$$

where $s^E$is the elasticity coefficient for constant electrical field E, T the mechanical stress, d the piezoelectric tensor. The rank 2 tensors for strain S and stress T, as well as the rank 4 tensor of the elasticity coefficients can be described in the Voigt notation [12].

2.1.2 Slip stick linear actuators

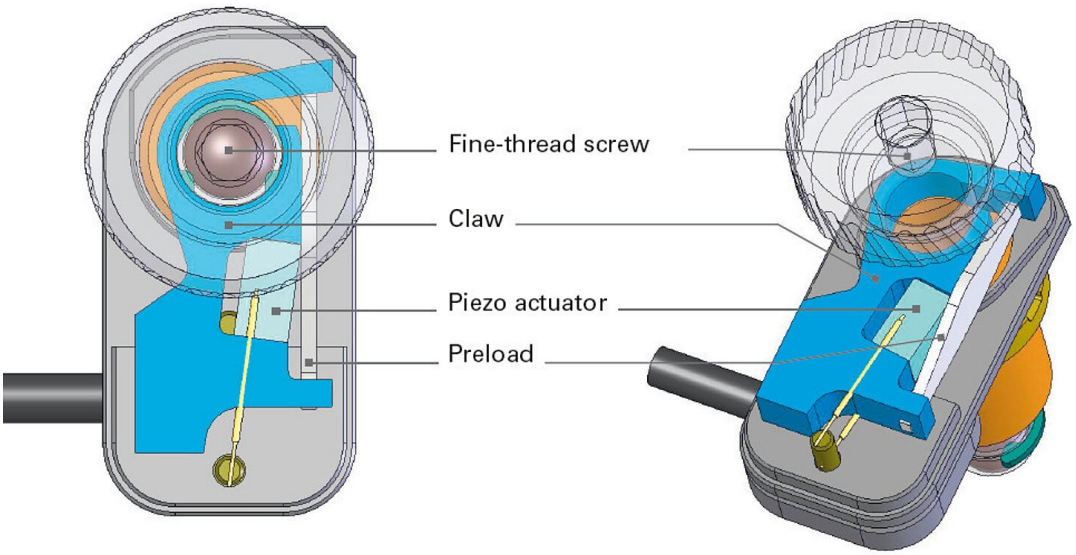

Figure 2.1: Schematic graphic of the PiezoMike motors. To actuate the mount the piezos rotate a claw, which in turn grips into the fine-thread screw, which is rotated. Upon the sharp voltage slope the claw slips around the screw, thus leaving it in place at the new position. Image taken form [13]

For our application in the optical dipole trap, we aim to achieve an alignment precision of 1 µm with regard to the trap position. The PiezoMike piezo motor mounted in MDI mirror mounts from Radiant Dyes is one of the options that fulfills our expectations. The PiezoMikes apply a slip stick principle. Figure 2.1 illustrates the inner workings of the PiezoMike. This means the piezo will slowly expand to push the claw, that grips into the screw, into the new position. Then the piezo rapidly contracts to its origin state. The claw gets pulled back swiftly, causing it to slip along the screw, thus leaving the

screw in the new position. The expansion of the piezo during this pulse, of course, has some hysteresis. However, as the whole sequence of expanding and retracting can be considered as one singular step, the displacement on repeated steps will always be (mostly) similar. The motor can be controlled with an external control device which outputs a saw tooth signal [8]. This enables doing multiple steps consecutively. Rotating the screw in backwards direction works analog to the forward step. Now the controller will apply a reverse saw tooth signal, which inverts the order to first expanding and slipping and then contracting and sticking. [13]

According to the data sheet of the Radiant Dyes PiezoMike motors [7], the linear actuators have a step size of 20 nm. As the screws in the mirror mounts are mounted in a distance of (30 ± 2) mm to the rotation axis this corresponds to a tilt of

$$\theta = \arctan\left(\frac{20\,\text{nm}}{(30 \pm 2)\,\text{mm}}\right) = (0.67 \pm 0.04)\,\mu\text{rad}. \tag{2.2}$$

This angle will be measured experimentally in the following section.

The control unit that was used is the E-870.4G PIShift Drive Electronics by Physik Instrumente [14]. The device is meant for slip stick piezo actuators, so the output is always saw-tooth voltage ramps, but the maximum voltage is adjustable. The voltage of the saw tooth signal can range from 0 to 100 V with a current of up to ±650 mA. Our model allows for control of up to four actuator. It is possible to address the PIShift driver via python commands, which is great for automated tasks, but also via a GUI, where one can adjust all the settings of the saw tooth signal and can control every actuator with the accuracy of a single step by the push of a forward or backward button. [8]

2.2 Step characterisation of piezo motorized mirrors

Before installing the mirror mounts in the main experiment, characterizing the behavior of the piezo motors was necessary. Our goal was to see, if the motorized mirror mounts are accurate and reliable enough to use for the optical trap in our main experiment. Furthermore we were interested in how consistent the mirrors are and if there is some hysteresis present. For this, we decided on a simple setup shown in figure 2.2(a), where we use a lens with focal length of 300 mm, the same as in our optical trap, to focus the laser onto a camera, while we use the motorized mirror to scan over a small range of angles.

The angle of the mirror tilt can be calculated from the figure 2.2(b) using the small angle approximation as

$$\theta = \frac{\arctan(d/f)}{2} \approx \frac{d}{2f}. \tag{2.3}$$

To measure the step size of the piezo motors, we used a python script that tilts the mirror by one step at a time, meaning that the piezo will get a single saw tooth peak, and then takes an image of the new position. To determine the position of the laser spot on the camera, a two dimensional Gaussian fit was used, as well as the known pixel size of the camera. Doing this for 12000 times in both forward and backwards direction, we get the result shown in figure 2.3. A linear fit of the type $\theta = a + b \cdot n$ was used to get the average step size, where θ is the tilt of the mirror, b the size of a single step and n the total number of steps in one direction. a is an arbitrary offset.

As we can see, there is a strong linearity in the position values with R^2 values of over 0.9999 , as well

[1] While in the sketch the angle is indeed 45°, it can be chosen arbitrary and does not affect the measurement of the angle θ

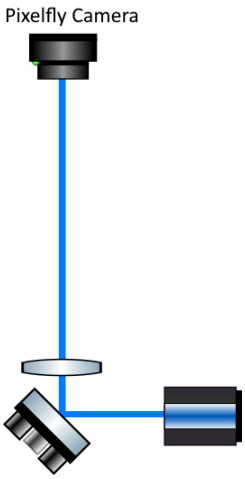

(a) Schematic of the measurement setup

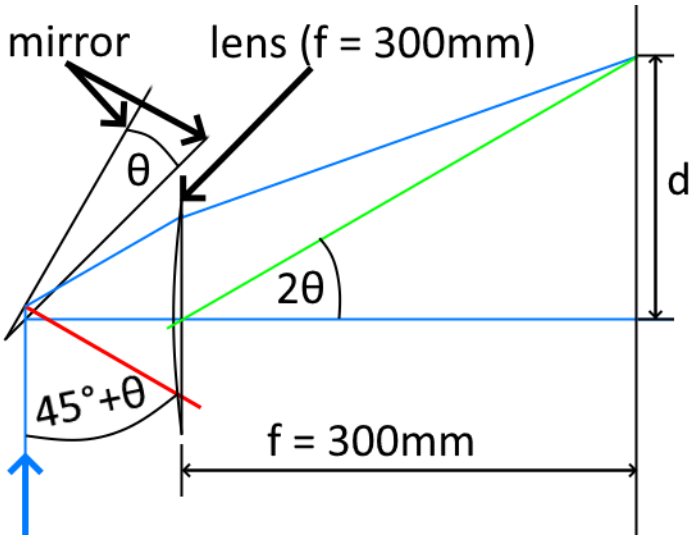

(b) sketch for the angle calculation

Figure 2.2: (a) Shows the setup we decided on using, while (b) shows a not to scale sketch for the angle calculation. The mirror gets tilted by an additional angle θ from the reference angle of 45° [1]. The green auxiliary line is parallel to the refracted laser after hitting the tilted mirror. d is the distance on the camera chip.

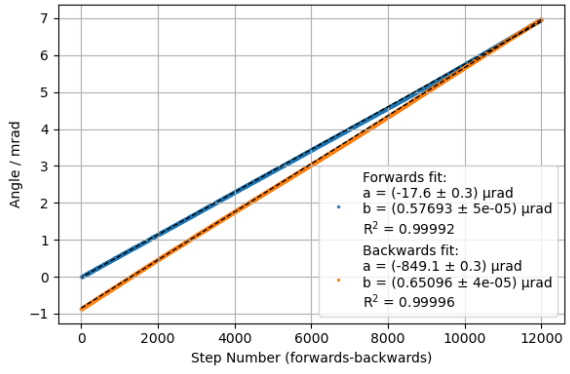

(a) Mirror tilt and fits for 12000 consecutive steps - first forwards (blue) then backwards(orange)

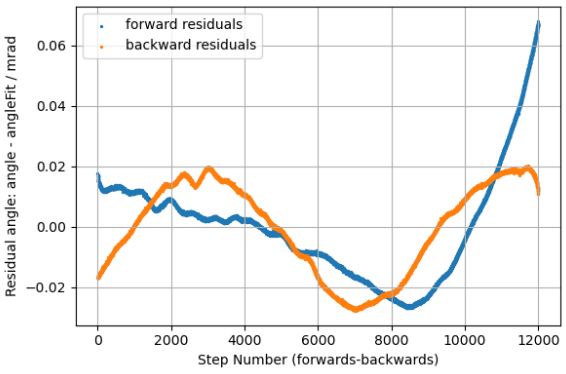

(b) Residuals of the linear fit for the mirror tilt

Figure 2.3: (a) shows the largely linear behavior of the piezo motors albeit some offset between forward and backward direction, (b) The residuals show some small non linearity

as barely any hysteresis. Looking at the residual plots in figure 2.3(b) one can see some smaller wobbles, as well as a larger underlying deviation. The smaller wobbles are likely caused by dust on the camera chip, lens or filters, which can cause newton rings and will interfere with the Gauss fits. While the overall hysteresis is small, with it being less than 1% of the total movement, when looking at the smaller frame between 10000 and 12000 steps forwards, it can change the movement by about 0.06 mrad per 2000 steps. This would amount to a change in step size by about 0.03 µrad or 5% of the measured step size. The cause of this hysteresis is unclear. While it seems to be somewhat position dependent, there does not appear to be a clear periodicity. One Idea, what might cause this, are some irregularities with the screw, for example an uneven thread, but it might also just be environmental changes like temperature drifts. While the fitting error for b is in the order of 10^{-4} smaller average slope, this does not represent the actual accuracy with which we can predict the size on an individual step. As the variation in the step size, can be seen to be up to 5% of the measured values, that is a good estimate for our error. On top of that we get the systematic error of the lens positioning, which is about (300 ± 10) mm or 3%, leading to a total error of 6%.

What we do see, is that there is a difference in slope between the directions of movement. This might stem from different behavior of the piezo under rapid versus slow expansion or contraction, for example through drift, as well as differences in the saw tooth signal generated by the control unit. According to the manufacturer of the PiezoMikes [13] a slight offset between forward and backward motion seems to also be expected with the backwards step size being slightly smaller than the forward step size. In our measurements the difference between step sizes, is not consistent between different piezo motors (see table 2.1) or settings (see table 2.2) and there was no clear trend, as to whether the forwards or backwards step is larger. Between the different motors the ratio between forward and backwards motion can be as little as 1% or up to 15 %. In section 2.3 we will showcase an option to compensate for the offset between forward and backward motion.

Serial Number	b_{fw}/ µrad	R^2_{fw}	b_{bw}/ µrad	R^2_{bw}	$b_{\mathrm{fw}}/b_{\mathrm{bw}}$
114048214	0.69 ± 0.04	0.99996	0.67 ± 0.04	0.999996	1.02 ± 0.09
114048205	0.58 ± 0.03	0.99992	0.65 ± 0.04	0.99996	0.89 ± 0.08
114048212	0.52 ± 0.03	0.99995	0.53 ± 0.03	0.999998	0.99 ± 0.08
114048209	0.93 ± 0.06	0.999994	1.00 ± 0.06	0.99997	0.93 ± 0.08
114048211	0.77 ± 0.05	0.99994	0.89 ± 0.05	0.99997	0.87 ± 0.07
114048207	0.57 ± 0.03	0.99995	0.66 ± 0.04	0.99997	0.85 ± 0.07
114048215	0.71 ± 0.04	0.999995	0.65 ± 0.04	0.999995	1.09 ± 0.09
114048206	0.56 ± 0.03	0.9998	0.56 ± 0.03	0.9997	1.01 ± 0.09
114048213	0.81 ± 0.05	0.999994	0.74 ± 0.04	0.999996	1.09 ± 0.09
114048208	0.53 ± 0.03	0.99998	0.54 ± 0.03	0.99997	0.97 ± 0.08

Table 2.1: The measured stepsize in forward b_{fw} and backward b_{bw} direction for all the tested piezo motors, the calculated R^2 from the fits and the ratio $b_{\mathrm{fw}}/b_{\mathrm{bw}}$ in between the forward and backward step size

In table 2.1 is a list of the stepsizes from the motors that were measured above. All the motors show a clearly linear behavior, and the step sizes range from (0.53 ± 0.03) µrad to (1.00 ± 0.06) µrad with the average between the measured values being at (0.678 ± 0.009) µrad. The average agrees within margin of error with the step size we calculated from the data sheet in equation 2.2. However some of the individual motors seem to vary by a lot more than we would expect from the spec sheet with the

maximum outlier having a step size 50 % larger than specified and the smallest outlier a stepsize 20 % smaller than specified. According to the Physik Instrumente company [13], the PiezoMike Linear Actuator, might experience a decrease in stepsize of up to 30% during their specified lifetime. Our piezo motors were in use before in a different function but it is unknown how frequently they were used, so this might already provide a suitable explanation for some difference in the step sizes. Furthermore, since the manufacturer already expects degradation over time to change the step size, it seems reasonable to assume, that they also allow for a larger manufacturing tolerance, which would offer another explanation for the larger outliers.

Voltage	step frequency	b_{fw}/ µrad	R^2_{fw}	b_{bw}/ µrad	R^2_{bw}	$b_{\mathrm{fw}}/b_{\mathrm{bw}}$
80 V	400 Hz	0.69 ± 0.04	0.99996	0.67 ± 0.04	0.999996	1.02 ± 0.09
60 V	400 Hz	0.49 ± 0.03	0.9998	0.43 ± 0.03	0.999995	1.13 ± 0.10
80 V	2 000 Hz	0.73 ± 0.04	0.99990	0.70 ± 0.04	0.999992	1.04 ± 0.09

Table 2.2: The step sizes measured for different parameter combinations for the PiezoMike with serial number 114048214.

We were also interested to see, if changing the settings has an influence on the behavior of the piezo motors. For this we qualitatively changed 2 settings (see table 2.2). First we lowered the maximum voltage of the saw tooth signal from 80 V to 60 V. As this equates to not running through the whole step cycle, but only doing a partial step, we expect to see a reduction in step size. This is exactly what we see, with the forward step size 29 % and the backward step size 36 % smaller than our original measurement. It would also be possible to decrease the voltage even further, but not unlimited so, as one soon runs into the point where the piezo does not turn the screw at all.

Second we tried to increase the step frequency from 400 Hz to 2 000 Hz. This caused a slight increase in the stepsize by 6 % forwards and 4 % backwards, but this is still within margin of error. It was speculated that this might be caused by the clamp, that is holding the screw, slipping further with the increased speed. As the effect is relatively small compared to the other deviations we observed, it can be mostly neglected for our use case. However, it might still be good to keep in mind, that changing the settings here can also affect the behavior of the motor.

2.3 Compensation for different step sizes

As shown in section 2.2, there is not only a difference in step size between forward and backward movement, but even more so between the different motors. And the measurements already show, that the step size of the piezo motors is suitable small, to precisely align optical setups by manually clicking on the forward or backwards button until optimal alignment is reached. To calculate the approximate position after moving an arbitrary amount of steps, one will have to count the total amount of steps in both directions and then multiply by the step size in the respective direction. Here we want to demonstrate that it is in fact possible to compensate for the difference between the motors and to move the laser spot in a controlled square path on the camera chip.

For this we utilized both the horizontal and vertical axis, by walking the beam in a rectangle pattern on the camera chip a total of 5 times. As a base measurement the mirror gets tilted 20 times by 50 steps in each direction for each square. So one square consists of 1000 steps in forward horizontal direction, 1000 steps in forwards vertical direction, 1000 steps in backwards horizontal direction and 1000 steps in

backwards vertical direction. This gets repeated 5 times. Based on the step sizes we measured in table 2.1, we can calculate the total angle that gets covered in each direction. By looking at the base row of table 2.3 we can calculate that the total offset we expect in horizontal direction after 5 loops is $\Delta\theta_x = (100 \pm 130)\,\mu\text{rad}$ and $\Delta\theta_y = (-350 \pm 110)\,\mu\text{rad}$ in vertical direction. The margin of error is with 130% rather large here, but that is to be expected, as the error adds up for each repetition of the square. As seen in figure 2.4(a) the observed drift is even larger, than anticipated with $\Delta\theta_x = (124 \pm 4)\,\mu\text{rad}$ and $\Delta\theta_y = (-435 \pm 13)\,\mu\text{rad}$, which corresponds to a relative deviation from our expectations of 24% for both axis. However, the measured drift is still within margin of error of our expectations.

When comparing the averaged measured total angle of the sides of the rectangle with the expectations, it becomes apparent, that while the measured angles match our expectations within margin of error, we are slightly underestimating our step size in the selected region. The measured angles are 2-7% larger than the expected values. It is also notable, that the largest difference between the sides occurs between the forward and up direction, with the total angle in forward direction being 19% larger that the angle in up direction.

	Direction	N	Calculated θ	Measured θ	$\theta_{\text{fw/up}}/\theta_{\text{bw/down}}$	$\theta_{\text{h}}/\theta_{\text{v}}$
Base	forward	$50 \cdot 20$	$(690 \pm 40)\,\mu\text{rad}$	$(712 \pm 15)\,\mu\text{rad}$	1.042	1.073
	backward	$50 \cdot 20$	$(670 \pm 40)\,\mu\text{rad}$	$(683 \pm 14)\,\mu\text{rad}$		
	Up(forwarad)	$50 \cdot 20$	$(580 \pm 30)\,\mu\text{rad}$	$(605 \pm 13)\,\mu\text{rad}$	0.871	
	Down(backward)	$50 \cdot 20$	$(650 \pm 40)\,\mu\text{rad}$	$(695 \pm 15)\,\mu\text{rad}$		
N_1	Forward	$36 \cdot 20$	$(496 \pm 30)\,\mu\text{rad}$	$(514 \pm 11)\,\mu\text{rad}$	1.012	1.044
	Backward	$37 \cdot 20$	$(496 \pm 30)\,\mu\text{rad}$	$(508 \pm 11)\,\mu\text{rad}$		
	Up(forwarad)	$43 \cdot 20$	$(498 \pm 30)\,\mu\text{rad}$	$(537 \pm 11)\,\mu\text{rad}$	1.013	
	Down(backward)	$38 \cdot 20$	$(494 \pm 30)\,\mu\text{rad}$	$(530 \pm 11)\,\mu\text{rad}$		
N_2	Forward	$14 \cdot 50$	$(483 \pm 29)\,\mu\text{rad}$	$(497 \pm 10)\,\mu\text{rad}$	1.012	1.067
	Backward	$14 \cdot 50$	$(469 \pm 28)\,\mu\text{rad}$	$(491 \pm 10)\,\mu\text{rad}$		
	Up(forwarad)	$17 \cdot 50$	$(493 \pm 30)\,\mu\text{rad}$	$(526 \pm 11)\,\mu\text{rad}$	0.996	
	Down(backward)	$15 \cdot 50$	$(488 \pm 29)\,\mu\text{rad}$	$(528 \pm 11)\,\mu\text{rad}$		
N_2	Forward	$14 \cdot 50$	$(483 \pm 29)\,\mu\text{rad}$	$(509 \pm 11)\,\mu\text{rad}$	1.018	1.050
	Backward	$14 \cdot 50$	$(469 \pm 28)\,\mu\text{rad}$	$(500 \pm 11)\,\mu\text{rad}$		
	Up(forwarad)	$17 \cdot 50$	$(493 \pm 30)\,\mu\text{rad}$	$(531 \pm 11)\,\mu\text{rad}$	1.0057	
	Down(backward)	$15 \cdot 50$	$(488 \pm 29)\,\mu\text{rad}$	$(528 \pm 11)\,\mu\text{rad}$		

Table 2.3: The calculated and measured angles for the discussed step variations. One can see, that there is a significant improvement in the ratio between forward and backwards direction for the variants N_1 and N_2 compared to the base variant. The ratio between hoizontal and vertical directions is smaller for all the N_1 and N_2 variations compared to the base variant, but only by less than 3%.

As a test, we selected two sets of values N_1 and N_2 for the amount of steps we take in each direction to get a good square with reduced overall drift. The value sets were calculated as follows in equation 2.4 and can be seen in table 2.3.

$$N_1 = \left\lfloor \frac{25}{b} \right\rfloor, \qquad N_2 = \left\lfloor \frac{10}{b} \right\rfloor \quad . \tag{2.4}$$

With the first set of Values, the path looks a lot more like a square with the horizontal side covering a

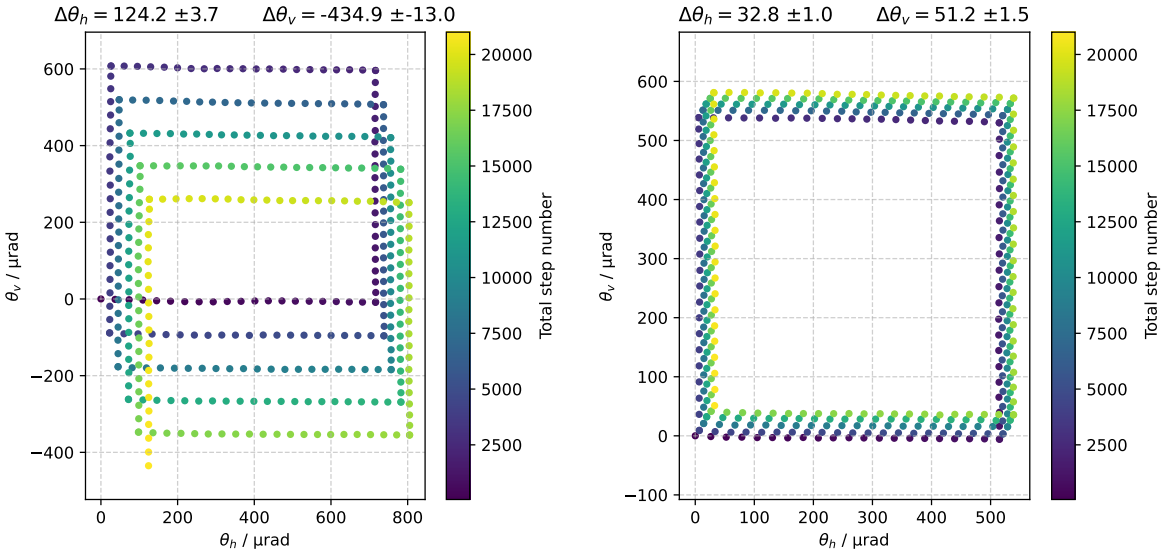

(a) Base Measurement

(b) N_1 Version

Figure 2.4: Comparison between uncompensated drift and compensated drift for square movements. The measured relative vertical mirror angle θ_{v} is plotted against the relative horizontal mirror angle θ_{h}. The displayed points turn from dark blue to yellow with the measurement progress.

average total angle of (511 ± 8) µrad and the vertical side covering (534 ± 8) µrad. The largest difference between the sides is here between up and backward direction by around 6%, which is reduced by 68% compared to the 19% ratio we observed without compensation. Furthermore the drift after 5 loops also gets significantly reduced to $\Delta\theta_x$ = (33 ± 1) µrad and $\Delta\theta_y$ = (51 ± 2) µrad which is a reduction by 73% and 88% while the covered angle in each direction only decreased by 12 - 28%.

The second set of values showed an even better result, with the drift being almost none existent, however the ratio between horizontal and vertical direction got slightly worse. The same measurement, at the same initial starting position, and also otherwise identical settings was repeated a few days later again. As one can see in figure 2.5(b), the values got worse overnight, despite not changing anything intentionally. This showcases just how external factors, such as room temperature, air current, etc. can have a significant influence on the behavior of the motors.

Thus, it can be concluded, that while it is possible to achieve near perfect results per coincidence as seen in in figure 2.5(a), we cannot assume that a precise calibration can be consistent over time. A calibration measurement that records the piezo motor behavior at different position does not seem useful, as there are too many changing variables. Instead we can look at our rough calibration measurement and approximate the step size with its 6% accuracy, but have to assume that the 6% are a calibration error, that will thus accumulate linearly.

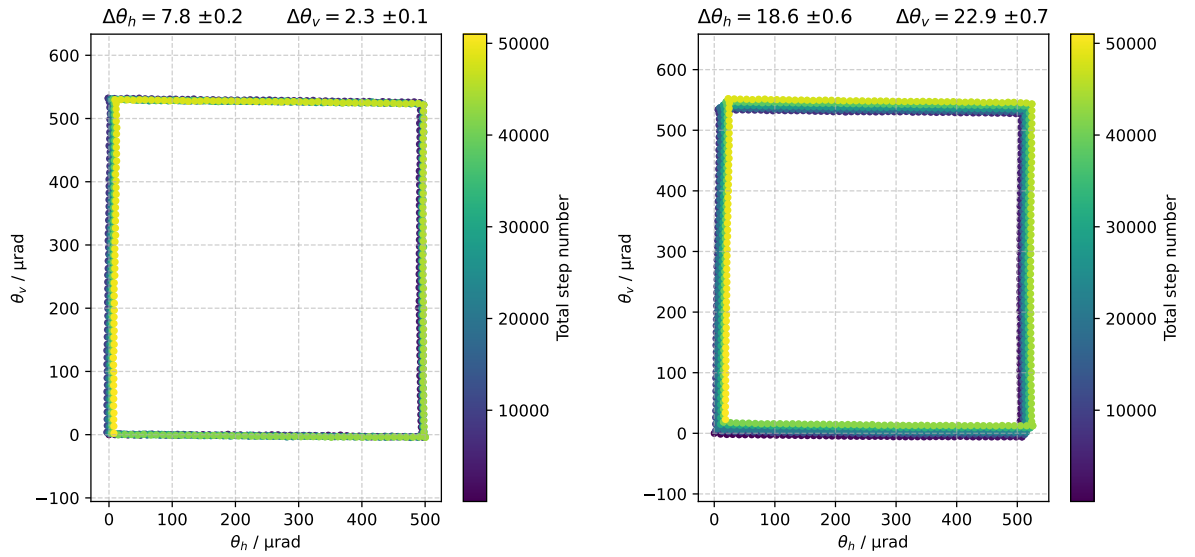

(a) N_2 version day 1

(b) N_2 version day 2

Figure 2.5: Comparison of the same square movement on two different days. The measured relative vertical mirror angle θ_v is plotted against the relative horizontal mirror angle θ_h. The displayed points turn from dark blue to yellow with the measurement progress.

2.4 Mirror mount stability

Before replacing the mirror mounts in the optical dipole trap of the main experiment, there was another concern. The ideal case for us would be a setup, that can be precisely aligned once, and then will remain in that position for an extended period of time. Thus we were interested in the pointing stability of the mirror mounts. Originally the piezo motors were installed in Radiant Dyes MDI mounts. Those mounts are the lighter version and possess 2 Springs, that hold the front plate in place. However there is also a high stable version of these mounts, that connect the front plate with 4 springs to a thicker back plate. In this section we will discuss the replacement procedure of the piezo motors into the new mounts and compare the stability of the two mount options.

Mirror mount replacement

The disassembly and reassembly process of the Piezo motors is very easy with the wrench shown in figure 2.6(c). First the small metal ring with the small indentations at the top gets loosened with the custom wrench. Then whole motor can be unscrewed from the mirror mounts. As one can see in figure 2.6(b), there is an outer thread and an inner threading that runs all the way through the outer thread and the motors. For reassembly the screws will be screwed into the new mounts and tightened again with the nut and the special wrench.

(a) Before disassembly

(b) Removed PiezoMikes

(c) PiezoMikes in new mount

Figure 2.6: Before and after images of the mirror mount replacement for the PiezoMikes

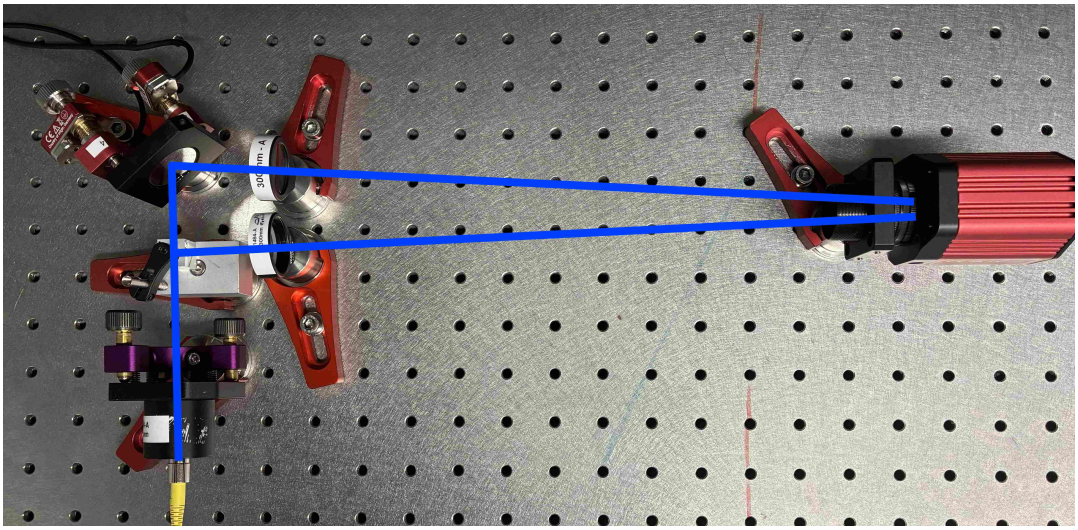

Figure 2.7: Photo of the stability measurement setup

Stability tests

For the stability measurment the following setup was used. From a fiber outcoupler the laser gets directed onto a non polarizing beam splitter cube, where one half of the beam gets focused onto the camera chip by a 300 mm lens. The other half of the beam hits the motorized mirror and is also focused, with a 300 mm lens, onto the same camera chip, but onto a different position. This enables us to individually evaluate both the reflected beam from the mirror as well as a reference beam. Using this setup we expect the only difference between the beam and reference to be caused by the mirror mounts we want to test. The setup can be seen in figure 2.7.

To make it easier to compare the stability, the position data acquired from the camera chip with two dimensional Gauss fits, was translated into the corresponding angle of the mirror tilt. From the reference beam (see figure 2.8(a)) we can already observe that there is some underlying drift, that appears to affect the whole system. To account for this, we used a quadratic fit, which will be used as an offset for the

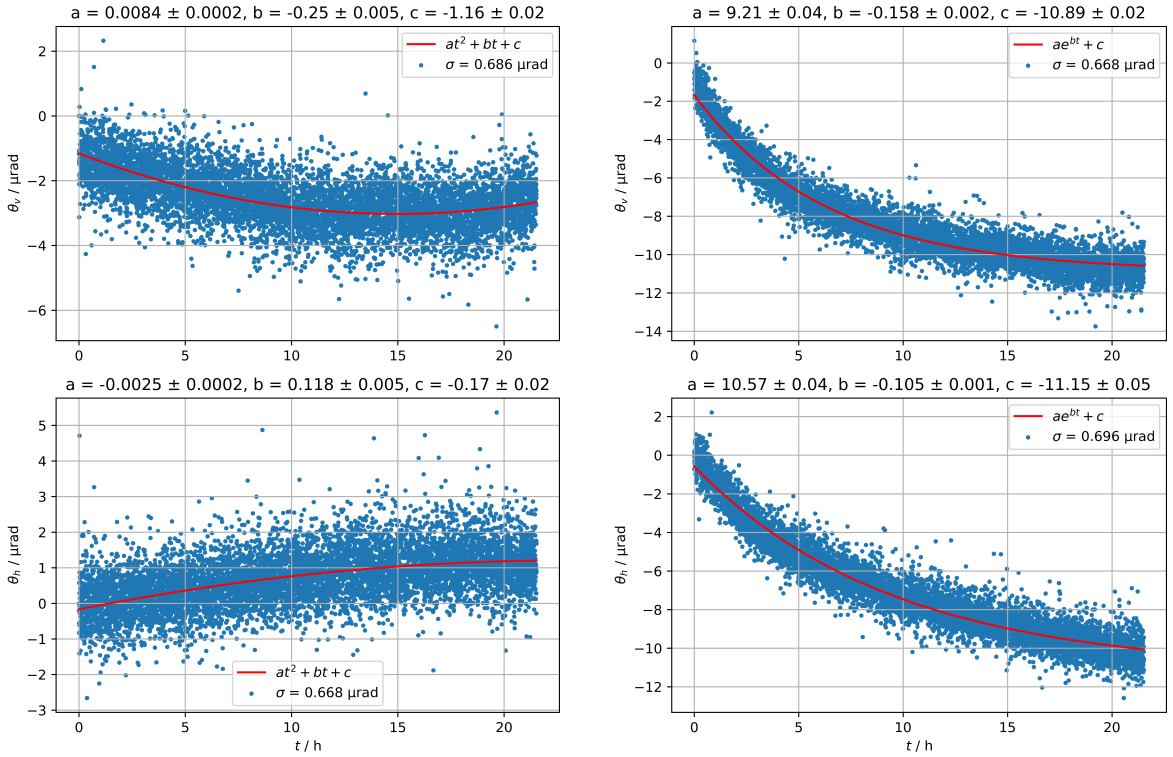

(a) reference beam

(b) Radiant Dyes MDI-PiezoMike mirror mount stability

Figure 2.8: (a) shows the pointing stability of the reference beam, (b) Shows the pointing stability of the older Radiant Dyes MDI-PiezoMike mirror mount. The background taken from the reference beam, was already removed from the data points. (a)(b) The upper plot shows the vertical angular position change, while the lower plot shows the horizontal angular position change. The angle refers to the tilt of the mirror.

mirror mount measurement. The remaining residual standard deviation gives us a reference value of the general noise in the measurement system, be it the camera, air currents, or other components that introduce fluctuations. Here, the residual standard deviation is between 0.67 and 0.69 µrad, meaning this is the resolution with which we can resolve our stability measurement of the mirrors.

Looking at figure 2.8(b), one can observe that the older MDI mirror mount with the piezo motors shows a significant drift in both axis that levels out over time. It is important to note, that the stability measurement was started a a few minutes after the mirror mounts were freshly installed in the stability measurement setup. The observed time period seems to correlate well with an exponential decay model. We can use this to get a measurement, of how long it will take for the drift to level out. The decay constants are $\lambda = -b = (0.105 \pm 0.001)$ 1/h and $\lambda = -b = (0.158 \pm 0.002)$ 1/h leading to a half life between 4 and 7 hours. The residual standard deviation is around 0.67 and 0.7 µrad in the same range as the reference beam. This shows that apart from the drift, there are no observable fluctuations, as we are limited by the general noise of our system.

For the Radiant Dyes MDI high stability mounts, the same procedure was followed, with the reference signal in figure 2.9(a) showing similar behavior to the first reference plots. The high stability mounts, however, behave different to the normal Radiant Dyes MDI mounts. For the vertical

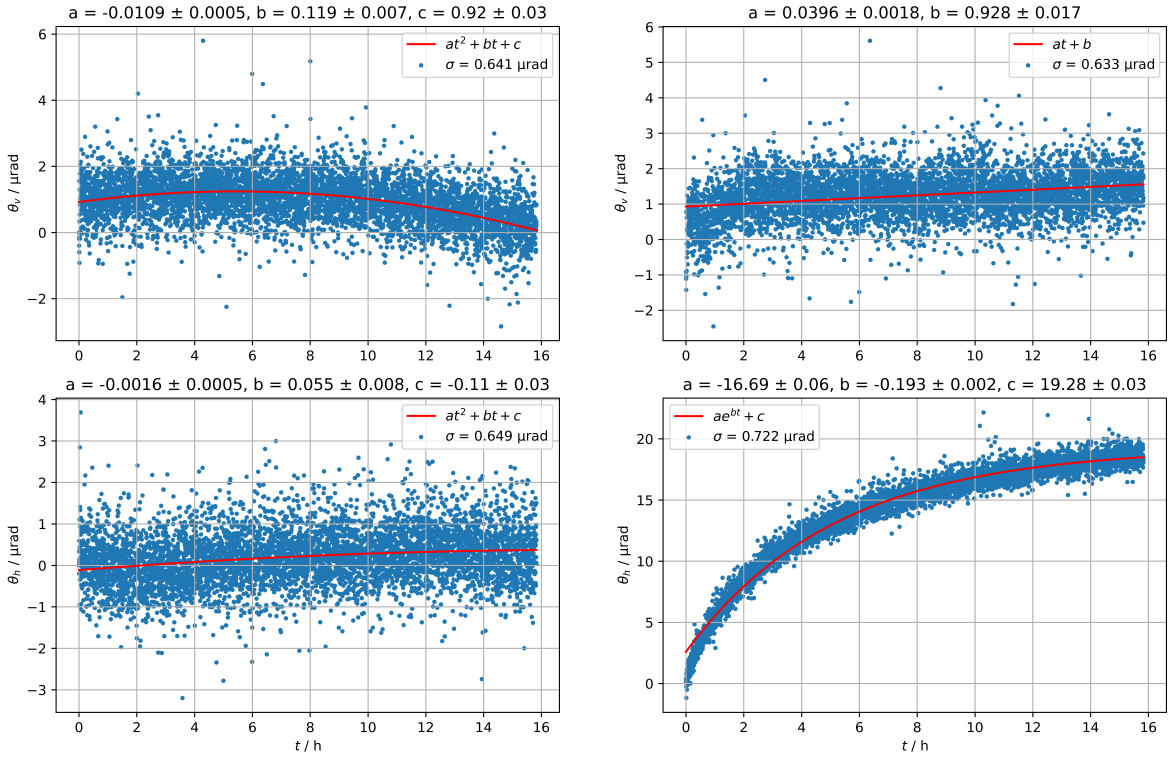

(a) reference beam

(b) MDI-high stability PiezoMike mirror mount stability

Figure 2.9: (a) shows the pointing stability of the reference beam, (b) Shows the pointing stability of the new MDI-high-stability-PiezoMike mirror mount directly after installation. The background taken from the reference beam, was already removed from the data points. (a)(b) The upper plot shows the vertical angular position change, while the lower plot shows the horizontal angular position change. The angle refers to the tilt of the mirror.

angle, there is barely any position change observable, with the a linear fit showing a total change of $\Delta\theta_v = 16 \cdot a = (0.634 \pm 0.029)$ µrad after 16 hours, this is still within our measurement tolerance. The horizontal angle, in contrast, shows a significant drift, that covers almost $\Delta\theta_h = 20$ µrad in 16 hours, but also levels out like the drift observed with the normal Radiant Dyes MDI mounts. The decay constant here is $\lambda = -b = (0.193 \pm 0.001)$ 1/h with a half time of 3.6 hours.

So far, this shows no clear indication that any of the mounts are more stable than the other in terms of the long term pointing stability, as both appear to show significant drift, at least directly after they were installed in the setup. We also looked at the stability of the Radiant Dyes MDI high stability mounts after already being installed for multiple days in the stability test setup. As figure 2.10 shows, there is no significant drift, with the linear fit suggesting a displacement of the horizontal angle after 16 hours of $\Delta\theta_v = 16 \cdot a = (0.522 \pm 0.020)$ µrad. The residual standard deviation is also at around 0.65 µrad comparable to the previous measurements.

To draw a conclusion with regard to the stability comparison, first consider, that the residual standard deviations of all the measurements (both reference and mirror) lie within same range of 0.65 to 0.7 µrad. This indicates, that any potential higher frequency fluctuations of the mirror mounts, cannot be resolved within the present measurement sensitivity. Instead we are limited by the system noise of

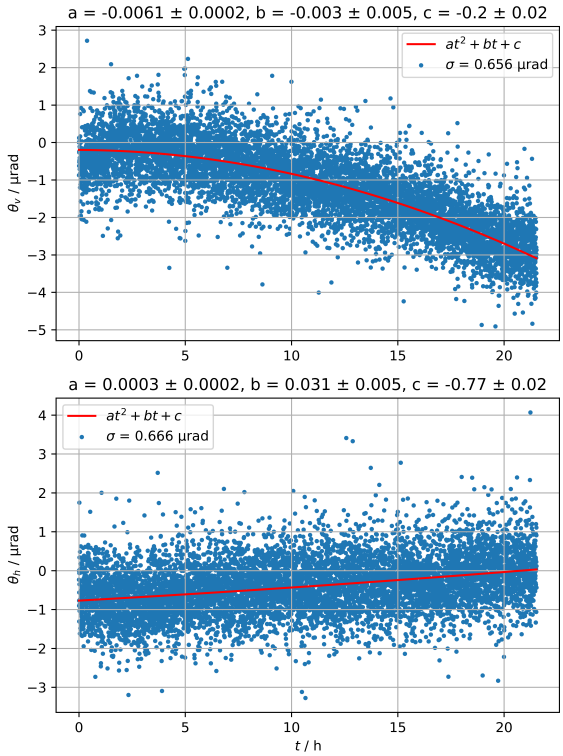

(a) reference beam

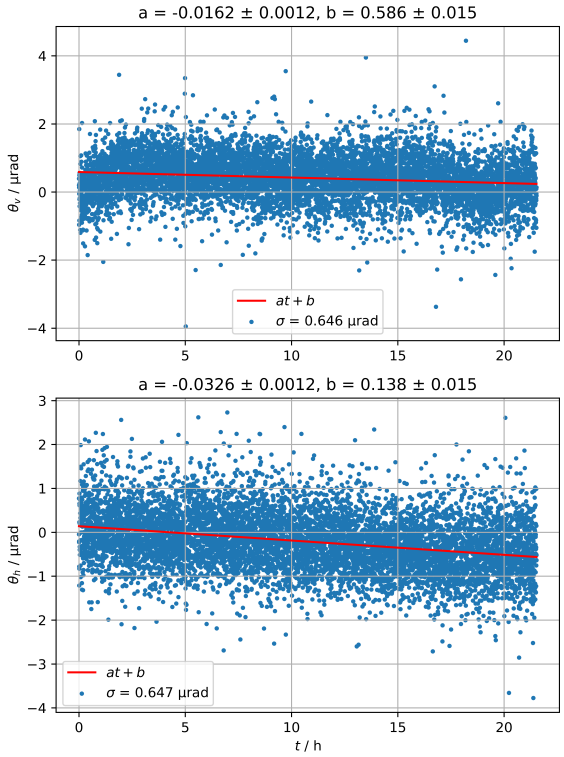

(b) Radiant Dyes MDI-high stability PiezoMike mirror mount stability

Figure 2.10: (a) shows the pointing stability of the reference beam, (b) Shows the pointing stability of the new Radiant Dyes MDI-high-stability-PiezoMike mirror mount in an undisturbed setting. The background taken from the reference beam, was already removed from the data points. (a)(b) The upper plot shows the vertical angular position change, while the lower plot shows the horizontal angular position change. The angle refers to the tilt of the mirror.

the experimental setup or other contributions like electronic camera readout noise. To meaningfully compare the mirror mounts in that regard, we would have to significantly reduce the system noise, or use an extended measurement setup, for example by introducing a telescope, to magnify the measured angle and thereby reducing the dependence on system noise. Overall, its reassuring, that the short term stability against fluctuations is better than the observed standard deviation and at least on the same order of magnitude as the step size of the mirrors.

Secondly we consider the overall significant drift we observed in the measurements for the first hours after the mirror mounts were installed. Here, it is important to mention, that the piezo motors have to be connected by a power cable. If this cable is not completely relaxed, a even a slight tension could generate a torque. This could either apply to the mount as a whole, or to the motors themselves. To compensate for this, it might be an option, to glue the outer threading into the mirror mounts, so that the screw cannot slip through the thread even marginally. When the mounts are installed in the main experiment, the alignment can be monitored with regular measurements and easily reproduced with the improvements offered by the motorized mirrors without touching the mounts by hand.

CHAPTER 3

Optical dipole trap

Optical dipole traps use the interaction, between the electric field of a far detuned laser light with the induced electric dipole moment of neutral atoms, to generate a conservative trapping potential. This interaction leads to a shift in the energy levels of the atom and is described by the AC-Stark shift. For small electric fields E and the eletrostatic polarizablity α_i for given S or P states, the stark shift is given by [4]

$$\Delta E_i^{\text{stark}} = -\frac{\alpha_i}{2} E^2 \quad . \tag{3.1}$$

The polarizablity is positive for red detuned light. As the energy shift is dependent on the laser intensity, a potential gradient can be generated by tightly focusing a laser beam. By adding a second focused beam, that crosses the first beam, the intensity at the intersection gets further increased, thus creating the deepest trapping potential at the crossing point. The Rubidium Rydberg Quantum Optics experiment utilizes such a crossed trap to hold a cloud of ultracold rubidium atoms. [15]

3.1 Setup

The optical trap in the RQO experiment uses a single laser source with 1 064 nm, that is reflected by two mirrors to form a cross. The optical setup in simplified form is shown in figure 3.1. The two beams are crossed in an 31.4° angle to each other. This updated setup contains two piezo-motorized steering mirrors, that will be used for the reproducible alignment of the optical dipole trap.

The incoming beam (in the figure left) is linear polarized. This is accomplished by the combination a half waveplate and a polarisation beamsplitter. The collimated beam then gets reflected onto the first steering mirror by a fixed alignment mirror. From the mirror the beam is focused by a 300 mm LA4579-1064 lens. As the design wavelength is not the one that is used, we expect a slightly longer focal length of 308 mm. The location of the optical dipole trap for the rubidium atoms is determined by the focal point. It is important to note, that the trapped atoms are inside of a glass cell with ca. 5 mm thick glass windows. This glass cell will cause a shift of the focus point, as well as an offset to the beam positions.

On the other side of the glass cell, the beam gets recollimated by a 200 mm LA4102-YAG lens. The focal length is again different for our wavelength with 205 mm. The beam then gets reflected by a fixed mirror towards the second steering mirror. From here, the beam is again focused by a second

200 mm LA4102-YAG lens. It is crucial, that both beam arms of the optical trap cross each other in their respective focal point, to receive an optimal trapping result.

In the the experiment sequence, the atoms are first laser cooled in a magneto-optical trap, and then transferred into the optical dipole trap. More information about the experimental sequences is given in previous theses [4][16]. The laser for the dipole trap is intensity stabilized to around 10 W by using an AOM. To avoid creating a standing wave pattern at the beam intersection, that would greatly increase the atomic loss, the linear polarisation of the second arm of the optical trap is rotated by 90°. This is accomplished with the combination of half wave plate and quarter wave plate before the second steering mirror (not shown in the figure). After the beam comes out from the optical trap it is then redirected into a beam dump and a photo diode, that is used for the power stabilisation.

3.2 Simulation of 3D trap movement

Gaining understanding, how adjusting the available degrees of freedom affects the hole system is a huge benefit, to both the manual alignment process and a necessary requirement for automatic alignment procedures. And while path tracing of simple optical components can also be done by hand, when adding a multitude of optical components and looking at beam paths in the three dimensional space, this requires a thorough investigation.

For this simulation the `optiland` python package was used [6]. The package uses ray optics to calculate 3D raytracing and allows surfaces with any refractive index to be placed at any place in space. This allows us to meticulously recreate the setup in the python simulation. Such a recreation is shown in figure 3.1. In order for the beam path to be traced correctly all surfaces must be added in the correct order and for lenses with the correct distance between front and back plane. The first surface will always need the refractive index of the material, while the second surface gets the refractive index of air. It was also accounted for the fact, that the mirror mounts will not rotate the mirrors directly around their center, but slightly offset by 15 mm. This is important, as that will cause a small, but noticeable position change of the mirror, when it is tilted. To accomplish this, the center of the object, around which gets rotated, undergoes a shift by the offset in both vertical and horizontal direction.

For our simulation we were of course interested in the point of maximum intensity. This point is usually located at the crossing point of the two beams, so finding the crossing point of the simulated beams was crucial. This proved to be a slight challenge, as the package provides no surface objects, that contain the position data of the traced rays. The solution for this was found by directly creating an internal rays object, that would also normally be used to create the figures. But now we can use that to extract the position data of the rays and to calculate the crossing point.

In figure 3.1 the setup that was described in section 3.1 is shown, how it was implemented for the python simulation. All core components, that affect the beam path, such as mirrors and lenses, as well as the windows of the glass cell were regarded. The only thing left out are the half- and quarter wave plates, as they are approximately perpendicular to the beam path and will not have a significant influence to it. One might notice, that the steering mirrors appear to be not hit in the center, but that is caused by the way optiland handles its objects and the fact, that the center point of the mirror was moved to accommodate for the correct behavior when tilting the mirror. The figure showcases, that the beams can be aligned in a way, that they cross each other in their respective focus point.

Figure 3.2 shows how the position of the crossing point between the two dipole trap beams changes, when the steering mirror 1 gets tilted in the horizontal direction. One can see, how the position change

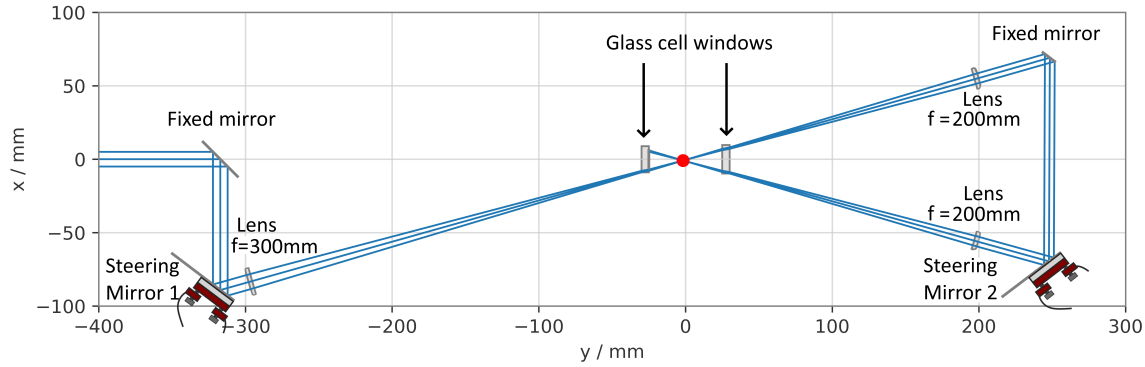

Figure 3.1: Simulation of the optical trap beam path with python. The crossing point is represented by the red dot. The incoming beam is represented by three parallel rays, that are focused in the crossing point. The figure was labeled slightly edited for better visibility. The axis labels correspond to the coordinate system used to describe the experiment [4].

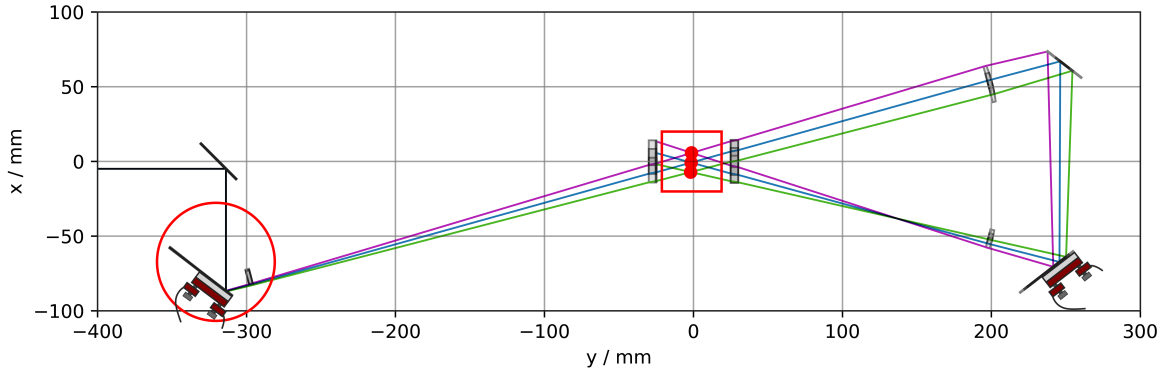

Figure 3.2: Simulation of three different angles of the steering mirror 1 (in the red circle). The purple, blue, and green lines each illustrate the laser beam path for a specific mirror tilt. For purple, blue and green the mirror is tilted by θ = (-10, 0, 10) mrad respectively.

in direction of the y axis gets compensated by the mirrors and lenses behind the glass chamber. Thus the focus point moves mainly along the x axis. When tilting the second steering mirror, the first arm of the optical trap remains stationary, so the focus point will move in a straight line following the first arm.

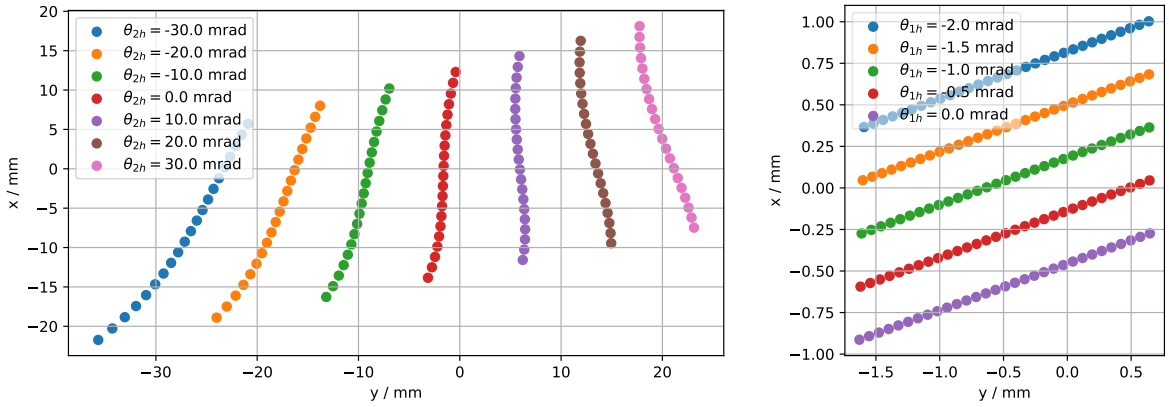

(a) larger scale

(b) detailed excerpt

Figure 3.3: Simulation of the crossing point between the two arms of the optical trap in dependence of different horizontal angles for both steering mirrors. (a) The angle of the first mirror is changed, while the second mirror is kept fixed at an angle θ_{2h}. The first mirror covers a range of $\Delta\theta_{1h} = 40$ mrad in 2 mrad steps, while the second steering mirror is positioned in 7 discrete angles θ_{2h}. (b) The second mirror is tilted, while the first mirror is kept at a fixed position θ_{1h}. The first mirror is positioned in 5 discrete angles θ_{1h}, while the second steering mirror covers a range of $\Delta\theta_{1h} = 3$ mrad in 0.1 mrad steps.

We will now look in more detail how the focus point changes with different angles of the two steering mirrors. For this we will only look at the position change inside the area of the red square. First the angle of the second steering mirror is kept fixed, while we iterate the first mirror over an angle range of $\Delta\theta_{1h} = 40$ mrad. This gets repeated for multiple angles of the second mirror. In figure 3.3(a) we show a rather large range of points, and cover a huge area compared to the dimensions of the atom cloud in the RQO experiment. The shown dimensions are displayed for demonstration purposes and are not comparable to our optical trap, as the trap position will only be changed by small distances smaller than 1 mm. This means, for the observable region of interest we expect an approximately linear behavior.

When looking at the red line of points in figure 3.3(a) for $\theta_{2h} = 0$ mrad close to the origin of x and y axis, the movement is almost exclusively in the x axis, while the y axis remains mostly constant. However, when looking at the more extreme angles, we observe a significant share of the movement in the y axis as well. If we were to observe this movement along the y axis, this does not mean, that the optical trap itself is bad, but that the angle of the fixed mirror and the steering mirror 2 does not match. So it does tell us that the angle of the two arms of the optical trap is not symmetrically aligned with our laboratory coordinate system.

In figure 3.3(b) we show a smaller excerpt of angles, that is close to the range in which we will align the optical trap. Here the focus lies on the movement of the second steering mirror. Therefore, the angle of the first mirror remains fixed, while the angle of the second mirror gets iterated over a range of 3 mrad. As before, this gets repeated for 5 different angles of the first steering mirror. As one can see, the crossing point follows exactly along the beam path of the first arm of the optical trap in a linear manner. This is precisely how one would expect it to be. Also for different angles of the first steering mirror, the

rays are spaced in an even and nearly parallel manner which is something we will use in section 3.4 to calculate the ratio between the angle tilt of the first steering mirror and the position change of the crossed optical trap.

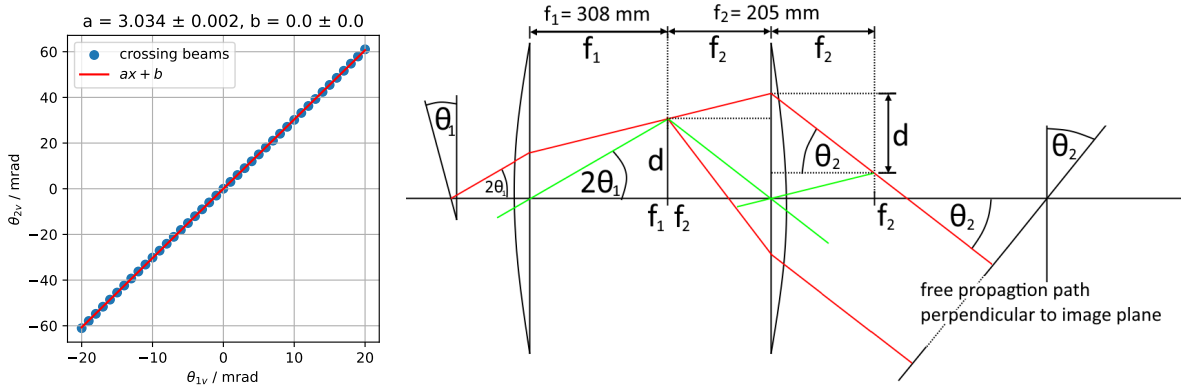

(a) Simulation

(b) path diagram

Figure 3.4: (a) Shows the relation between the horizontal angles θ_{1v} and θ_{2v} of the two steering mirrors necessary to maintain a crossing point between the two beams. (b) Exaggerated path diagram looking at the optical trap from the side. The setup is equivalent to a telescope, but the second lens represents two different lenses with the same focal length. With the small angle approximation the angle θ_2 can be expressed in terms of θ_1 with $\tan(2\theta_1) = \frac{d}{f_1}$ and $\tan(\theta_2) = \frac{d}{f_2}$ as $\theta_2 = \theta_1 \cdot \frac{2f_1}{f_2}$

So far, we considered the mirror rotation in horizontal direction. Now, rotations in vertical direction will be discussed. When one of the steering mirrors gets tilted in vertical direction, the arms of the optical trap move apart from each other and lie in a different plane. For example if the first mirror gets tilted such that the beam gets deflected upwards, the second steering mirror will also have to point upwards to compensate for the introduced angle. As one can see in figure 3.4(b) the optical trap works similar to a telescope setup. With the simplified assumptions from the path diagram we expect the ratio between the two angles of the mirrors to be

$$\frac{\theta_{2v}}{\theta_{1v}} = 2 \cdot \frac{f_1}{f_2} = 2 \cdot \frac{308\,\text{mm}}{205\,\text{mm}} \approx 3.005 \ . \tag{3.2}$$

To confirm this with with the simulation, we iterated over a range of $\Delta\theta_{1v} = 40\,\text{mrad}$ and then used the `minimize_scalar` from `scipy.opitmize` to find the crossing point again. As one can see in figure 3.4(a) the results of a linear fit show a ratio of 3.034 ± 0.002 which differs only by 1% from our initial estimate. The ratio between the angles needed for compensation is of course heavily reliant on the lens positions. So given a good enough knowledge of the mirror angles, one could use this ratio to check the lens alignment in the real experiment.

3.3 Installing the new mounts in the main experiment

In the previous sections 2.2-2.4, the mirror mount performance was characterised and we now understand how the trap position changes, when the mirrors are tilted (section 3.2). Based on these insights, it

was decided to install the normal MDI mirror mounts with the PiezoMike piezo motors into the main experiment. For the realignment of the optical trap, we made use of the fact, that we already had a working dipole trap, by placing irises in front of every lens in the setup.

First the second steering mirror was replaced, as that way we would still have one arm of the dipole trap left as orientation in our imaging. Also the alignment of the second arm in vertical direction is way less sensitive to the whole system compared to the first arm. It was also noticed, that the profile of the motorized mirror mounts is slightly larger compared to the polaris mounts, so the posts, where the mounts were placed upon, had to moved backwards by a few millimeters to maintain the same position of the mirror as before. For the realignment process, we first optimized the intensity with the irises, that were placed to note down the previous beam path, using a power meter. For this the GUI of the PIShift driver was used. There, a plateau of the highest power was found with a range of around 1000 steps in both the vertical and horizontal axis. The crossed optical trap was then found again, by moving the second arm in the vertical axis by 50 steps at a time.

In preparation for the exchange of the first steering mirror additional irises were placed in the beam path. The same procedure was followed again. First the mirror had to be adjusted, so that the beam goes nicely through all the irises. Then the power of the beam running through the irises was optimized with a power meter by adjusting the beam position with the piezo motors 100 steps at a time. Replacing the first steering mirror, one has to be a bit more careful, as the alignment of the whole optical trap gets influenced by the first mirror position. For example, when tilting the first mirror in the vertical axis upwards, the first arm of the optical trap will move up, but at the same time this will cause the second arm of the optical trap to shift downwards by the same amount, the first arm just moved up. By tilting the first steering mirror upwards 50 steps at a time, the crossed optical trap was quickly found again.

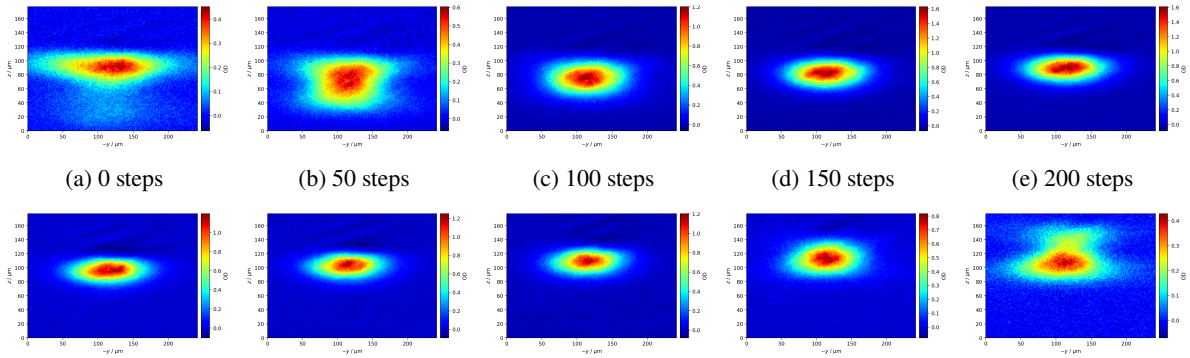

(a) 0 steps (b) 50 steps (c) 100 steps (d) 150 steps (e) 200 steps

(f) 250 steps (g) 300 steps (h) 350 steps (i) 400 steps (j) 450 steps

Figure 3.5: (a - j) show the imaging of the vertical plane of the atom cloud. The MOT loading time was increased to 2 seconds to load more atoms and to have a better contrast on the images. The second steering mirror is being tilted up by 50 steps per image.

To show, what finding the crossed optical trap looks like, we positioned the second arm of the optical trap just below the range of the atom cloud. Then we took a series of 16 averaged images and moved the second arm of the dipole trap up by 50 steps. This corresponds to a position change of the beam in the region of the crossed trap by $d = 50 \cdot 2 \cdot \theta f = (11.9 \pm 0.6)\,\mu\text{m}$ according to the mirror calibration. Looking at figure 3.5 one can follow the progress, of the two arms of the optical trap combining to a single crossed optical trap and them moving apart again. In image 3.5(a) the atoms are mainly trapped in

the single first arm of the optical trap, while the second arm can be barely made out below the atom cloud. Then in image 3.5(b) both arms begin to merge to a large atom cloud. Following images 3.5(c) to 3.5(i) both beams appear to nicely combine to a single focused crossed optical trap. Through this range the second arm covers 300 steps which corresponds to ca. 71 µm. It is difficult to compare the estimated change of the beam height with the images, as the atoms are mainly present in the overlap of the two beams. In image 3.5(j) the two arms begin to separate again, with the atoms being visible in both arms.

After successfully installing the new mirror mounts in the optical trap setup and finding the crossed optical trap again, we took some images of the atom cloud. In figure 3.6 both the vertical and horizontal imaging is displayed. In the horizontal plane the arms of the optical trap become visible in a lighter blue color than the background, while the atom cloud sits at the cross section of the two beams. In the vertical plane, the beams of the optical trap are behind each other, so there is only one line in addition to the atom cloud visible. The lasers themselves are not visible, but rather there are a few atoms, that are not trapped in the cross section but in one of the arms of the trap.

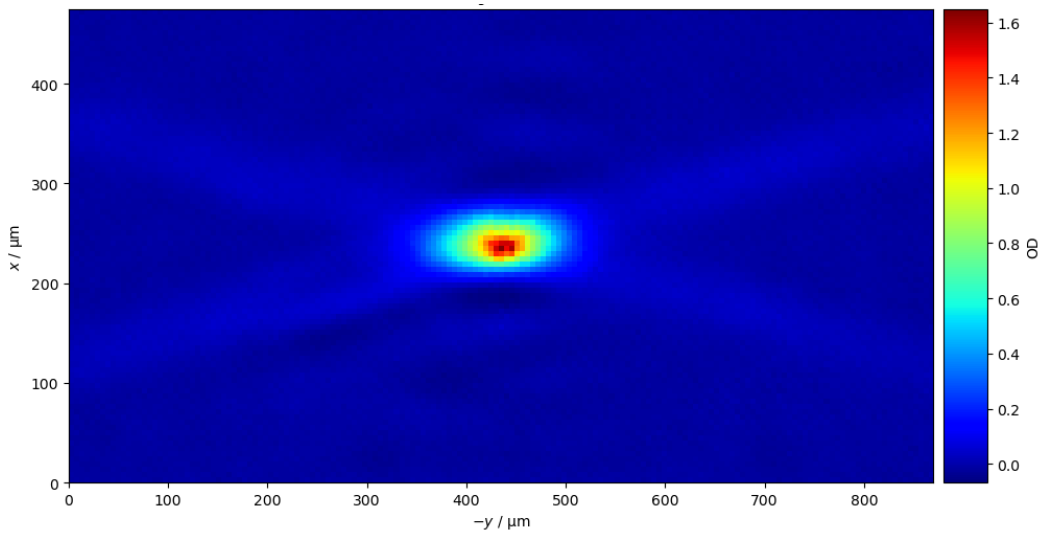

(a) imaging of the horizontal plane

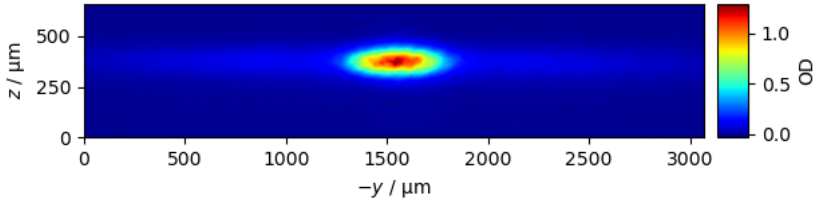

(b) imaging of the vertical plane

Figure 3.6: Images of the rubidium atom cloud in the crossed optical trap with 1 minute MOT loading time averaged over 300 images

3.4 Final tests in the main experiment

From the simulation shown in figure 3.3(b), we know, that the position of the atom cloud should only change in x direction, when the first steering mirror is tilted in horizontal direction. With this knowledge, we can calculate, by how much the cloud will move per horizontal angle of mirror tilt. To start, we remember how the relative angle θ of the mirror translates to a position offset d perpendicular to the optical axis in the focus point of a lens (see section 2.2). Hereby is $f = 308\,\text{mm}$ the effective focal length of the lens.

$$d = \tan(2 \cdot \theta) \cdot f \tag{3.3}$$

The focal length of the lens is at least 2 orders of magnitude larger than the displacement $d << f$ and the angle of the mirror tilt is small. This allows the assumption, that in the region of interest, the beams before versus after tilting the mirror are approximately parallel to each other. Using the sketch in figure 3.7, we can calculate the relative position change ΔX in the x direction in relation to the angle between the two arms of the crossed optical trap $\Phi = 31.4^\circ$ as

$$\Delta x = \frac{d}{\cos(\Phi/2)} = f \cdot \frac{\tan(2 \cdot \theta)}{\cos(\Phi/2)} \ . \tag{3.4}$$

By inserting the known values for f and Φ and applying the small angle approximation for θ, we can calculate the position change Δx per angle θ.

$$\frac{\Delta x}{\theta} \approx \frac{2 \cdot f}{\cos(\Phi/2)} = 0.640\,\mu\text{m}/\mu\text{rad} \tag{3.5}$$

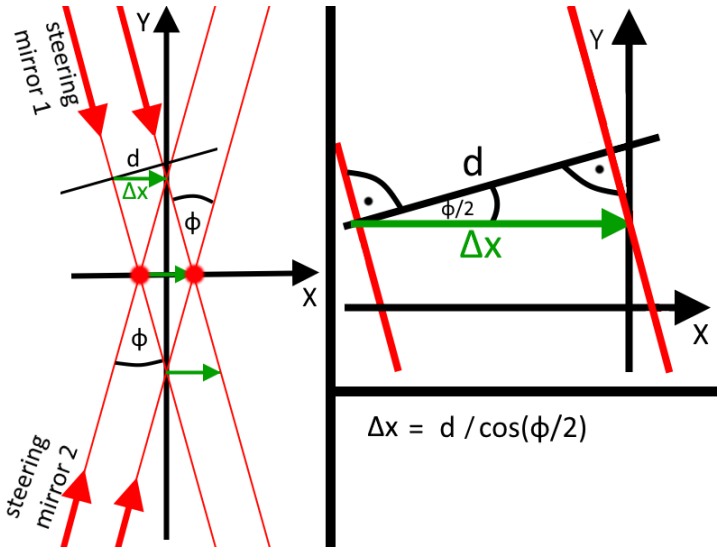

Figure 3.7: (left) The crossing point gets moved to the right indicated by the green arrow. This affects both beams which stay approximately parallel to each other in the region of the crossing point. The angle of the crossed optical trap Φ does change in principle, but for small θ this can be neglected. (right) The right angled triangle used to calculate the position change in x direction.

To compare this result with the real experiment, the atom cloud was imaged at various angles of the

first steering mirror. The relative tilting angle of the mirror was calculated using the total amount of steps and the results from table 2.1. The positions of the atom cloud were extracted using Gauss fits over summed optical density in x and y direction respectively. Then, the positions were plotted against the relative mirror tilt and a linear fit was performed to extract the ratio between the position change and the relative angle (see figure 3.8). The resulting slope is

$$\frac{\Delta x}{\theta} = 0.56\,\mu\text{m}/\mu\text{rad}. \tag{3.6}$$

It is important to note, that the error of the slope in 3.8 is only the fitting error, while we encounter calibration errors for both the horizontal imaging, as well as the step size of the piezo mirrors. Our result has a relative deviation, compared to the calculation of 12%.

In figure 3.8(b) the extracted positions of the y axis are shown. There are two outliers, who lie apart a total of 8 µm, while the other values are all at the same position within their margin of error. The performed linear fit, shows a trend of

$$\frac{\Delta y}{\theta} = (0.015 \pm 0.011)\,\mu\text{m}/\mu\text{rad}. \tag{3.7}$$

This is about 37 times smaller than the relative position change in x direction, so the assumption that the cloud only moves in x direction can be confirmed.

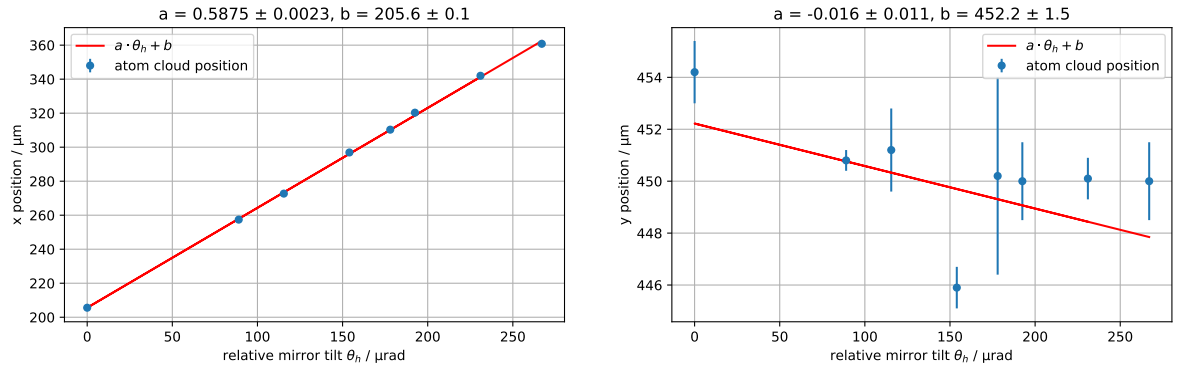

(a) x axis

(b) y axis

Figure 3.8: (a) Shows the measured relation between x position change and horizontal mirror tilt of the first steering mirror. (b) The cloud position in the y axis remains, barring some variance, in the same region for different horizontal angles of the first mirror

CHAPTER 4

Conclusion and outlook

During this thesis, new piezo motorized mirror mounts for the precision alignment of the optical dipole trap were tested and installed. Additionally a simulation of the optical trap position was conducted.

In the second chapter the details of the PiezoMike linear actuators were discussed. The actuators use piezo motors with a slip and stick principle. They are installed in Radiant Dyes mirror mounts and can tilt the mirror in two axis by a typical step size of 0.67 µrad. This was confirmed by our measurements. It was also observed, that the step size may vary between different piezo motors of the same type by up to 50% from the typical step size. To accommodate for the different step size, a rough calibration was performed, that allows to predict the tilt of the mirror within 6% margin of error. Overall it is possible to tilt the mirror to any position with submicroradiant accuracy within normal angular range for screw actuated mirror mounts.

With regard to the stability of the mirror mounts with piezo motors, the normal MDI mounts from Radiant Dyes were compared to their high stability version. Here, the standard deviations of the extracted beam positions did not differentiate between the reference beam and the beam reflected by the mirrors with motorized screws. This indicates, that high frequency fluctuations were not resolvable by the utilized measurement setup, as the position noise was dominated by the overall system noise. In conclusion the short term pointing stability was measured to be better than $\Delta\theta = \pm 0.7$ µrad for both versions of the mirror mounts. In terms of the long term stability, there is a significant drift observable, after the new installation of the mounts in an optical setup, that levels out within a day. We expect, that after mount relaxation, there will be no significant drift.

In the third chapter, the alignment of the optical trap was discussed. With the help of a python simulation, the position of the crossing point was analysed with regard to different combinations for the angles of the mirror tilt. Most notable here, is that the horizontal tilt of the first steering mirror will almost exclusively adjust the trap position along the x axis of our experiment. For the vertical alignment both steering mirrors can be used in combination to shift the trap location up or down. Hereby, the second steering mirror has to be tilted by thrice the amount of the first steering mirror to compensate for otherwise occurring vertical divergence of the beams.

To mark the successful conclusion of this project, the mirror mounts of the optical dipole trap were replaced with the piezo motorized steering mirrors. It was possible to confirm, that the first steering mirror does indeed only change the atom cloud position in direction of the x axis and it was found, that the observed position change in relation to the angle change matches predictions based on the simulation up to a relative deviation of 12%.

Outlook

With the successful installation of the motorized mirrors in the main experiment, the long term stability remains the most prominent point for debate. Here it will be necessary to monitor the behavior in the optical trap for the coming months to determine if there are recurring issues. It might be worth considering, to glue the outer threading of the piezo motors into the mirror mounts, to permanently remove one degree of freedom.

While the short term stability of the mirror mounts seems to be a non issue, it would still be interesting to get an accurate measurement of the whole system noise of the dipole trap. This could be used to decide if there is further room for improvement of the stability of the dipole trap. As a first test it might be possible to monitor the position of the beam from the optical trap after it exits the the glass cell for the second time.

For the dipole trap simulation, there are also options to improve upon the information gained. By adding a calculation of the beam waist, it would be possible to get accurate values for the beam overlap at the crossing point and for intensity profiles. This might offer some insight into how the alignment of the dipole trap affects trap depth and size of the atom cloud. Finally the result could be used to find a better optimization of the dipole trap or to create an optimized algorithm for automated alignment.

Bibliography

[1] I. Rakhmatulin, D. Risbridger, R. M. Carter, M. D. Esser and M. S. Erden, *A review of automation of laser optics alignment with a focus on machine learning applications*, Optics and Lasers in Engineering **173** (2024) 107923, ISSN: 0143-8166, URL: https://www.sciencedirect.com/science/article/pii/S0143816623004529.

[2] Z. Dong et al., *Structural stability design of an optical mirror mount adjustment mechanism*, Appl. Opt. **62** (2023) 9291, URL: https://opg.optica.org/ao/abstract.cfm?URI=ao-62-35-9291.

[3] R. Grimm, M. Weidemüller and Y. B. Ovchinnikov, *Optical dipole traps for neutral atoms*, 1999, arXiv: physics/9902072 [physics.atom-ph], URL: https://arxiv.org/abs/physics/9902072.

[4] H. M. Gorniaczyk, *Single Photon Transistor mediated by electrically tunable Rydberg-Rydberg Interactions*, PhD Thesis: Universität Stuttgart: Universität Stuttgart, 2016.

[5] L. P. D. Ahlheit, *Collective Rydberg Excitations in Magic Traps*, PhD Thesis: Rheinischen Friedrich-Wilhelms-Universität Bonn: Rheinischen Friedrich-Wilhelms-Universität Bonn, 2022.

[6] K. Harrison and contributors, *Optiland's documentation*, URL: https://optiland.readthedocs.io/en/latest/ (visited on 20/01/2026).

[7] *PiezoMike Linear Actuators*, URL: https://www.radiant-dyes.com/PDF/2018/Piezo_Mike.pdf (visited on 11/01/2026).

[8] *Technical Note E-870 PIShift Drive Electronics Models with a Case*, Physik Instrumente (PI) GmbH & Co. KG, 2014-06-24.

[9] R. J. Singh, *Solid State Physics*, eng, Pearson India, 2011, ISBN: 933251481X.

[10] A. M. Rudolf Gross, *Festkörperphysik*, eng, 4., uberarbeitete, aktualisierte Auflage edition., De Gruyter Studium, De Gruyter, 2022, ISBN: 3110782642.

[11] *Fundamentals of Piezo Technology*, URL: https://www.physikinstrumente.com/en/expertise/technology/piezo-technology/fundamentals (visited on 12/01/2026).

[12] S. Germer, *Interfacing Rydberg Atoms with a High Overtone Bulk Acoustic Wave Resonator on an Atom Chip*, Masters's Thesis: Rheinische Friedich-Wilhelms Universität, 2025.

[13] *PiezoMike Linear Actuators*, URL: https://www.physikinstrumente.com/en/expertise/technology/piezoelectric-drives/piezomike-linear-motors (visited on 23/12/2025).

[14] *PI Datasheet E-870 PIShift Drive Electronics Models with a Case*, Physik Instrumente (PI) GmbH & Co. KG, 2015-08-21.

[15] D. A. steck, *Quantum and Atom Optics*, eng, revision 0.16.6, 2025, URL: http://steck.us/teaching.

[16] N. Stiesdal, *Collective atom-light interactions with Rydberg superatoms*, PhD Thesis: University of Southern Denmark: University of Southern Denmark, 2022.

List of Figures

List of Tables

Acknowledgements

I would like to thank Prof. Hofferberth for giving me the opportunity to work on the RQO experiment during my bachelors thesis. I would also like to thank Prof. Linden for agreeing to be my second appraiser.

It is important for me to thank the people from the RQO group. Especially Daniil, who supervised my work in the lab and showed great guidance and Nina who showed me around the institute and always had an open ear for my questions even after leaving the group. Matthias, who started with me, and whom I had many fun hours in the lab and Lukas, who first showed me the experiment and finalized my decision to do my thesis in the NQO group.

I would also like to thank all of the members of the NQO group, who welcomed me into the group and whom I had a great time with during the group events such as the institutes Christmas party or the group breakfasts.

Finally I would also like to thank my family for their support.